Characterization of the local charge environment of a single quantum dot via resonance fluorescence

Disheng Chen, Gary R. Lander, Kyle S. Krowpman, Glenn S. Solomon, and Edward B. Flagg

Phys. Rev. B **93**, 115307 — Published 14 March 2016

DOI: 10.1103/PhysRevB.93.115307

Characterization of the local charge environment of a single quantum dot via resonance fluorescence

Disheng Chen,[1] Gary R. Lander,[1] Kyle S. Krowpman,[1] Glenn S. Solomon,[2] and Edward B. Flagg[1,*]

[1] *Department of Physics and Astronomy, West Virginia University, Morgantown, WV 26506, USA*
[2] *Joint Quantum Institute, National Institute of Standards and Technology, & University of Maryland, Gaithersburg, MD, USA.*

(Dated: February 22, 2016)

We study the photon-statistical behavior of resonance fluorescence from self-assembled InAs quantum dots (QDs) as a function of the density of free charge carriers introduced by an above band-gap laser. Second-order correlation measurements show bunching behavior that changes with above-band laser power and is absent in purely above-band excited emission. Resonant photoluminescence excitation spectra indicate that the QD experiences discrete spectral shifts and continuous drift due to changes in the local charge environment. These spectral changes, combined with tunneling of charges from the environment to the QD, provide an explanation of the bunching observed in the correlations.

I. INTRODUCTION

Indistinguishable single photons are potentially important in a number of quantum information processing applications, for example linear optical quantum computation[1], entanglement swapping[2–4], and quantum repeaters[5,6]. Indistinguishable photons are those with identical properties (*e.g.*, wavelength, bandwidth, polarization), which allows them to demonstrate Hong-Ou-Mandel interference[7]. Semiconductor quantum dots (QDs) have been shown to be good sources of single photons[8–10], and photons emitted from the same QD in rapid succession have been shown to have very high indistinguishability when the QD is in an optical cavity[11,12] or is excited resonantly[13]. Photons spaced more widely in time and those from separate QDs, however, do not show the same degree of indistinguishability[14–16] due to the inhomogeneous distribution of photon energies emitted by one QD state at different times. This inhomogeneous distribution is called spectral diffusion, and it is likely caused by fluctuating occupation of charge traps in the environment of the QD[17–22]. In order to produce indistinguishable single photons, the causes of spectral diffusion must be investigated and mitigated. One step in this process is to measure the dynamics and the influence on the QD of fluctuating charge traps in the environment.

The subtle fluctuations of the local electric field environment modify the energy levels of the QD through the quantum-confined Stark effect because of the QD's large DC electric polarizability. Spectroscopically, this effect manifests as a discrete jump, continuous drift or spectral broadening of the QD's absorption and emission lines depending on the relative position of the charge traps and characteristic time of the electric fluctuations. A charge trap close to a QD will result in a discrete shift of the peak in the QD absorption spectrum when the trap's occupation state changes. A single trap far from a QD will have an unnoticeable effect on the QD by itself, but a change in mean occupation of a large ensemble of traps will cause a continuous drift or broadening of the QD spectrum. In this study, we show that all of these effects are present in one QD's excitation spectrum when its local environment is perturbed by above band-gap optical excitation.

To resolve the fine change in the QD energy levels, we use resonant photoluminescence excitation (RPLE) spectroscopy, which measures the absorption spectrum by collecting the total resonant fluorescence from the QD using different excitation wavelengths. The resolution of this technique is solely dependent on the linewidth of the excitation laser, which is ∼1 MHz in our case. RPLE spectra with additional variable-intensity above-band excitation illustrate discrete spectral jumps in the QD resonance due to Stark shifts caused by nearby occupied charge traps. The number, relative position, and average occupation of the nearby charge traps can be deduced from the data. No electrical contacts are necessary as the measurement is entirely optical. Second-order correlation measurements of the emitted fluorescence show photon bunching that characterizes the time-scale of the charge trap dynamics. We found that the switching rate of the charge traps between occupied and unoccupied configurations increases by five orders of magnitude with increasing above band-gap excitation power even below the threshold where the above-band excitation produces photoluminescence (PL) on its own.

II. SAMPLE AND EXPERIMENTAL SETUP

The sample consists of InGaAs self-assembled QDs grown in the center of a 4-λ GaAs spacer between two AlAs/GaAs distributed Bragg reflectors (DBRs) with 14 and 20.5 periods on the top and bottom, respectively. The DBRs form a planar microcavity with a transmission mode from 923 $\sim$ 930 nm and a waveguide mode that confines light within the plane of the sample. The thickness of the GaAs spacer that defines the cavity is 1.06 um, leaving the QDs more than 500 nm away from either DBR. As discussed later, this relatively large dis-

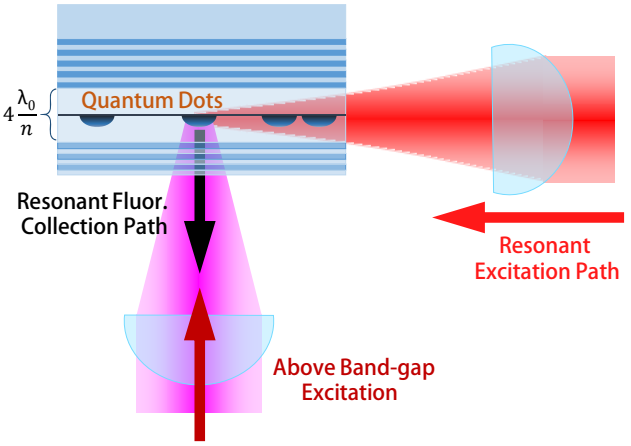

FIG. 1. Quantum dot sample with optical excitation and collection geometry. The resonant laser is focused on the cleaved face of the sample in order to couple into the waveguide mode of the cavity. The fluorescence is collected normal to the sample surface. The above band laser at 633 nm is focused through the collection lens onto the QD location. λ_0 is the cavity resonance wavelength in vacuum (930 nm) and n is the refractive index of GaAs (~ 3.5).

tance rules out the possibility that the observed discrete Stark shifts in the RPLE data are caused by charging of defects at the hetero-interfaces or the sample surface. The sample is maintained at 5 K in a closed-cycle cryostat. The optical excitation and collection scheme is depicted in Fig. 1. Laser light resonant with a QD transition is introduced into the waveguide mode of the sample via free-space coupling from the side; the QD is approximately 100 μm from the cleaved sample edge. When the QD transition is resonant with the cavity mode, the fluorescence is preferentially directed normal to the sample surface where it is collected by a 0.5 NA aspheric lens. The resonant excitation is provided by either a tunable continuous-wave (CW) diode laser or a mode-locked Ti:sapphire laser with a pulse length of 2.1 ps. Simultaneous with the resonant laser, an above band-gap excitation laser with a wavelength of 633 nm can be introduced normal to the surface. The fluorescence is directed through a 0.75 m spectrometer and thence either to a TE-cooled CCD camera or through an exit slit to a time-correlated single-photon counting (TCSPC) system. The second-order correlation function, $g^{(2)}(\tau)$, of the CW-excited fluorescence is calculated from the time-tagged photon detection data.

III. EXPERIMENTAL RESULTS

A. Time-Resolved Fluorescence

The QD lifetime T_1 is obtained from time-resolved fluorescence measurements where the QD is resonantly excited by the pulsed laser and the fluorescence is directed to a single-photon counting module (SPCM). The pulse has an energy of 0.17 pJ and a bandwidth of 76 GHz in linear frequency. This is two orders of magnitude wider than the QD's ground state transition linewidth, and well covers the observed spectral shifts due to the charge traps. Figure 2 shows an example time-resolved measurement without above-band excitation. The data are fitted with an exponential decay convolved with the measured instrument response function of the SPCM. We measured resonantly excited time-resolved fluorescence for different powers of above-band excitation and extracted an average lifetime of $T_1 = (518 \pm 3)$ ps. The extracted lifetimes show no trend with increasing above-band excitation power (inset of Fig. 2). Coupled with additional measurements discussed below, this suggests that the lifetime is not affected by the fluctuations of the local charge environment.

B. Resonant Photoluminescence Excitation Spectroscopy

We use RPLE spectroscopy to quantify the discrete shifts and continuous drifts of the QD energy levels caused by both nearby and distant charge carrier traps. The capture rate of charge carriers at these traps is expected to depend on the local free charge carrier density, which is controlled by adjusting the power of an above band-gap laser through 6 orders of magnitude. For each power, two RPLE spectra with orthogonal de-

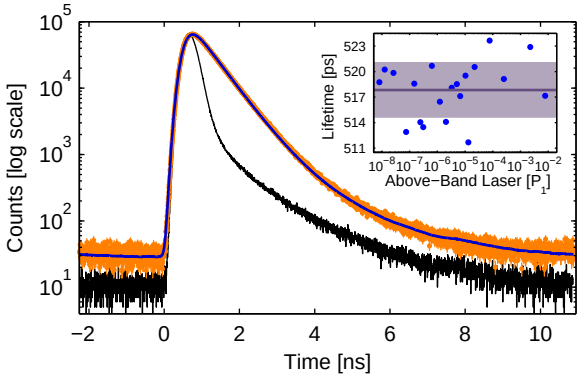

FIG. 2. (Color online) Time-resolved fluorescence from a single QD under pulsed resonant excitation and without above-band excitation. The data (orange dots) are fit by an exponential decay model convolved with the measured instrument response function of the SPCM (black curve). The blue curve is the convolved result. The inset shows the lifetimes extracted from similar time-resolved fluorescence measurements with different levels of above-band laser power represented as a fraction of the saturation power $P_1 = 28.5\mu$W. The lifetime varies little with above-band laser power, with an average value of $T_1 = 518 \pm 3$ ps. The average T_1 is depicted by the dark line in the inset, while the gray area is the standard uncertainty range.

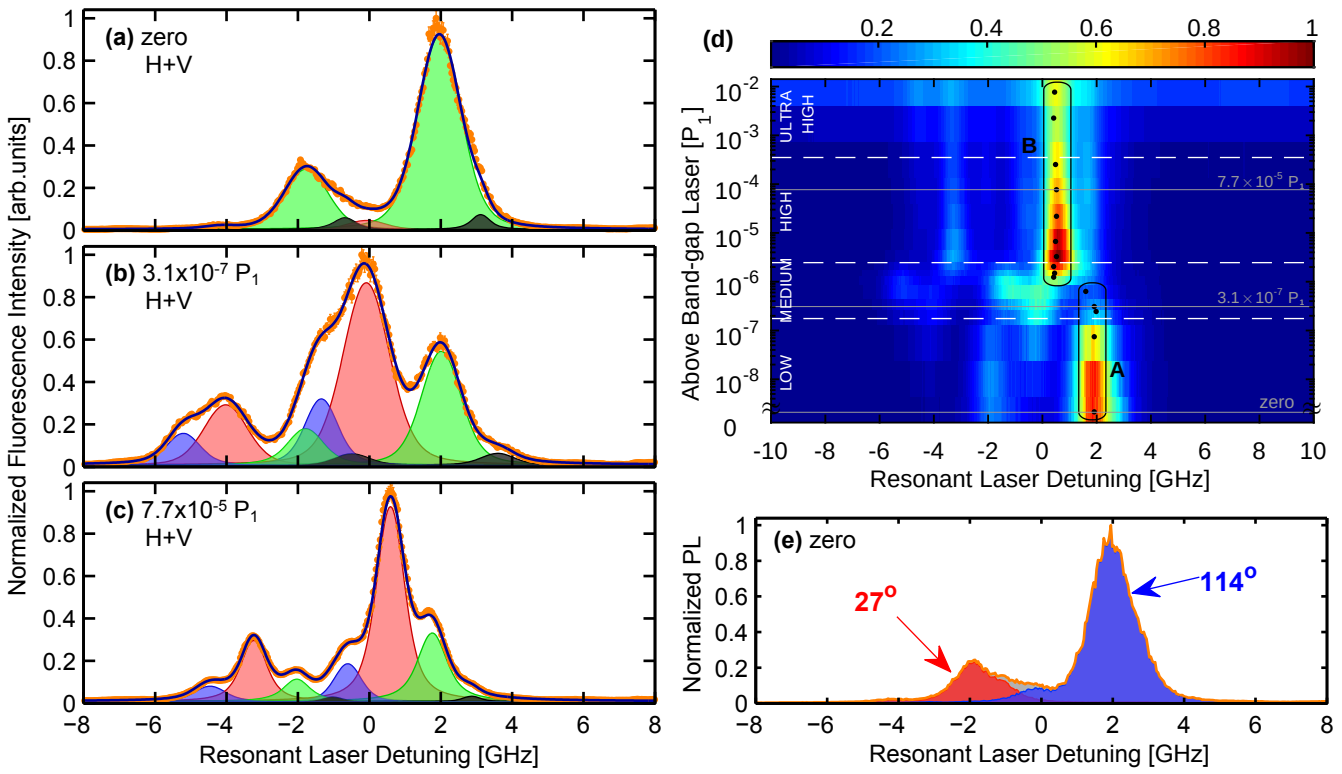

FIG. 3. (Color online) **(a)–(c)** Three examples of normalized resonant photoluminescence excitation spectra (RPLE) at above-band laser powers of zero, 3.1×10^{-7} P_1 and 7.7×10^{-5} P_1 respectively. The filled curves are the individual Voigt peaks used to do the fitting; the blue curve along the orange data points is the sum of these individual peaks. Zero detuning is defined as the middle point of the two Voigt peaks with largest amplitude (green) in (a), which corresponds to 928.3713 nm. Each curve is normalized to its own maximum. **(d)** 2D plot of 16 RPLE spectra taken at different above-band laser powers plotted in a logarithmic scale on the vertical axis. The color–scaled spectral intensity is normalized to the overall maximum of the measured fluorescence intensity. The grey lines denote the three spectra in (a), (b) and (c). The black dots are the positions where correlation data are collected. Box A denotes the data shown in Fig. 5(a) and box B those in Fig. 5(b). The white dashed lines indicate the boundaries for the different above-band power regimes. **(e)** An example of polarization-dependent RPLE without above-band laser. Two RPLE spectra were recorded using a linear polarizer oriented at 114° (blue) and 27° (red) from the horizontal. Their sum is displayed as the orange curve with grey filled area. The red and blue peaks are the same shape but displaced and with different amplitudes, which implies that the two peaks are the orthogonally polarized emission from the two fine structure split states of a neutral QD.

tection polarizations (H & V) are collected by scanning the frequency of a tunable 1 MHz bandwidth CW laser through the QD resonance at 10% of the saturation power $P_0 = 4.7\mu W$. The two spectra are then summed to give a final spectrum whose amplitude is proportional to the exciton population in the QD. In the summation, the polarization-dependent absorption due to the optics in the collection path is corrected.

Figure 3(a)–(c) shows three examples of summed spectra in three different power regimes of the above-band laser, *i.e.* low, medium and high power. Each spectrum is fitted with 8 Voigt profile peaks whose Lorentzian linewidth is restricted to be not less than the lifetime-limited value of 308 MHz in linear frequency according to T_1. Polarization dependent RPLE (Fig. 3(e)) suggests that these emission lines are from a neutral QD. Thus, 8 Voigt peaks gives 4 pairs corresponding to four different discrete Stark shifts (including the case where the shift is zero) experienced by the QD during the measurement.

We measured RPLE spectra for a number of QDs, and all those we surveyed showed either 1, 2, or 4 different Stark shifts. These are all powers of 2, which is consistent with an integer number of nearby 2-level charge traps. For example, two charge traps would result in $2^2 = 4$ different configurations. None of the QDs we surveyed showed 3 or 5 Stark shifts. Regarding the QD detailed here, to match the 4 discrete shifts observed in the RPLE data, the only possible trap arrangement is either two 2-level traps or one 4-level trap. Candidates for 2-level traps abound – for example, dopant impurities and other crystal defects – while to the authors' knowledge no 4-level traps have been reported in the literature. Thus we discard the latter possibility and conclude that there are two nearby 2-level charge traps influencing the QD. We denote the first trap as α, the second as β, and the possible trap configurations as $(\alpha\beta)$, where α, β can take

a value of 0 or 1 representing the empty (neutral) or occupied (ionized) state of each trap.

In Fig. 3(a)–(c), the 8 Voigt peaks are color coded into 4 pairs so that each pair stands for one trap configuration: the green peaks correspond to charge configuration (00), black peaks to configuration (01), blue peaks to configuration (10), and red peaks to configuration (11). Below we discuss the underlying reasoning for the assignment of these labels. There may be additional charge carrier traps far from the QD and randomly distributed, but their influences on the QD energies are limited. Their effect on the RPLE spectra is described by spectral line broadening, which consists of two parts: Gaussian widths of the Voigt profiles for inhomogeneous environmental broadening and additional Lorentzian widths for homogeneous non-radiative broadening. Due to the significant overlapping of multiple peaks in the spectra, the fitting is too ambiguous to distinguish these two sources definitively. But the Voigt line widths of all peaks are broadened by about a factor of 4 compared to the lifetime-limited value. Considering the relatively weak effect on the electric field at the QD from the free charge carriers and distant charge traps, the orientation of the asymmetry axis of the confinement potential of the QD will remain the same for all above-band powers. Therefore the amplitude ratio of the two fine structure peaks in each pair of Voigt profiles is constant for all above-band powers. We perform a global fitting of four spectra from different power regimes simultaneously to determine the ratios. Afterwards, each spectrum is fitted individually with the fixed amplitude ratios.

With no above-band excitation, one pair of peaks dominates the RPLE spectrum (the green peaks in Fig. 3(a)) showing that 83% of the time the traps are in the corresponding configuration. Without above-band excitation, the traps are expected to be in thermal equilibrium. If the traps are either shallow donor or acceptor impurities, in bulk GaAs at 5 K the fraction that are ionized is approximately zero. The fraction of ionized dopants near the QD may be increased by the proximity of the wetting layer quasi-continuum states, but it is still expected to be low. Therefore, we assign the neutral trap configuration (00) to the green peaks dominating the spectrum in Fig. 3(a).

At high above-band laser power we expect the free charge carrier density to be greater, and the charge traps correspondingly more likely to be charged compared to the case of low above-band power. Therefore, we assign trap configuration (11) to the pair of peaks that dominates the spectrum in Fig. 3(c), which is displayed in red. The other two configurations (01) and (10) are arbitrarily assigned to the black peaks which are shifted by about 1 GHz from the green, and to the blue peaks which are shifted by about –3 GHz from the green.

Figure 3(d) shows all 16 RPLE spectra at different above-band laser powers which span 6 orders of magnitude. We identify four regimes of above-band power based on the different patterns in the RPLE spectra:

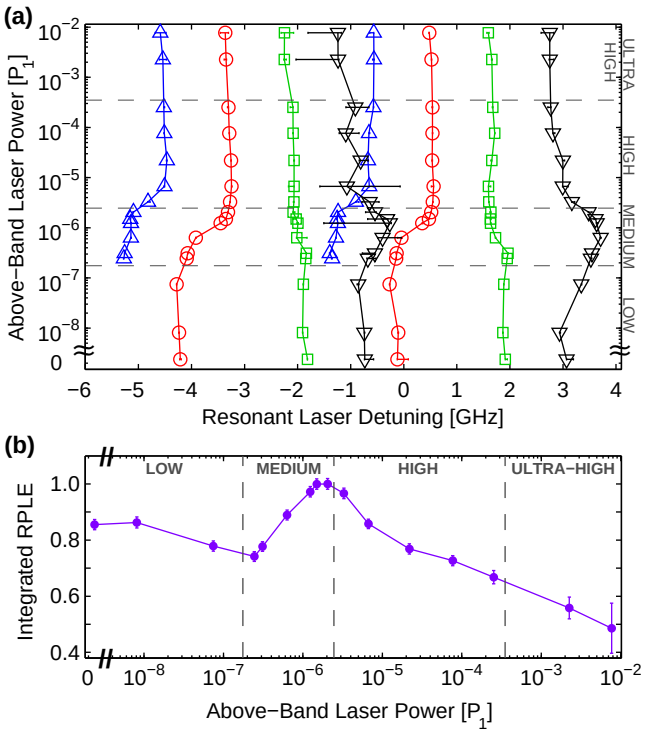

FIG. 4. (Color online) **(a)** Center detunings of resonance peaks. For the RPLE spectra that comprise Fig. 3(d), the center detuning of each Voigt profile in the fit is plotted versus the corresponding above-band laser power. The green square curve corresponds to trap configuration (00), the red circle for trap configuration (11), the blue up-triangle for trap configuration (10) and black down-triangle for trap configuration (01). The lines are guides for the eye. The horizontal dashed lines give the boundaries of different above-band power regimes. **(b)** Spectrally integrated intensity of RPLE spectra in Fig. 3(d). The baseline offset due to the above-band excitation has been subtracted so that the curve represents the emission solely due to resonant excitation; this effect is only significant in the ultra-high power regime. The error-bars correspond to experimental fluctuation and shot noise. The curve is normalized to its maximum value. The grey vertical dashed lines correspond to the boundaries of different above-band power regimes.

low power regime (zero $\sim 1.7\times10^{-7}$ P_1), medium power regime (0.17 P_1 $\sim 2.5\times10^{-6}$ P_1), high power regime (0.025 P_1 $\sim 3.5\times10^{-4}$ P_1) and ultra-high power regime (above 3.5×10^{-4} P_1). Note that even in the high end of the ultra-high power regime the above-band laser is less than 1% of the saturation power.

Figure 4(a) shows the best-fit Voigt peak positions of the spectra in Fig. 3(d). In the medium power regime, there is a continuous but quick peak shift of about ∼1 GHz for trap configurations (11), (01) and (10). This is possibly caused by partial screening of the electric fields of the trapped charges by the free charge carriers introduced by the above-band excitation. Fig. 4(b) shows the spectrally integrated RPLE of the QD as a function of above-band laser power. It reaches its maximum value

at 1.2×10^{-6} P_1, indicating that the local charge environment around the QD most favors neutral exciton emission (over trion or biexciton emission) at that power. When the above-band laser goes over this threshold, the QD fluorescence starts to decrease, reflecting the fact that more free charge carriers are available for the QD to capture in favor of trion and biexciton emission, which reduces neutral exciton emission. As the data shows, the QD resonant emission is suppressed by a factor of 2 in the ultra-high power regime compared to the maximum emission intensity at medium power.

All the RPLE peaks show a gradual spectral drift from the low power regime to the ultra-high power regime. This is possibly caused by an asymmetric distribution of many distant charge traps that are far from the QD. By investigating the evolution of the green peaks (configuration (00)), we determined the drift to be an approximately 0.6 GHz red-shift. This red-shift happens to follow the same trend of QD energy drift when the local temperature is increased by a small amount, about 0.2 K[23]. However, other dots show a blue-shift of similar amount over the same above-band excitation power range. Therefore, thermal heating by the laser is not sufficient to explain these observations. In addition, a calculation with a simple two-dimensional thermal conductance model with the maximum above-band power used here (thermal conductivity of GaAs at 4 K is 10 $W\cdot cm^{-1}\cdot K^{-1}$, and absorption coefficient at 633 nm is 4×10^4 cm^{-1}) shows that the temperature rise would be less than 0.2 mK. This is too small to account for the observed spectral shift.

C. Correlation Function of Resonance Fluorescence

The RPLE data quantify both the magnitude of the Stark shifts experienced by the QD and the time-averaged occupation probability of the charge traps that cause them. The time-dependent behavior of the charge traps can be characterized by the photon statistics of the resonance fluorescence. When the resonant laser is tuned to one of the peaks in the RPLE spectrum, the QD will emit strong fluorescence. If a nearby charge trap switches from unoccupied to occupied, or vice versa, the QD resonance will shift and the fluorescence intensity will be reduced. This effect manifests as bunching in the second-order correlation function of the fluorescence, $g^{(2)}(\tau)$, on the time scale of the trap switching rate.

Another effect that manifests as bunching in $g^{(2)}(\tau)$ is charging of the QD. In contrast with QDs in a diode structure[24–26], here the charge state of the QD in the sample is uncontrolled, and the QD may capture a charge from the environment. The resonant laser is tuned to the neutral exciton transition and when the QD is charged that transition is not available. Thus, when the QD is charged there will be no resonance fluorescence. The charged QD may capture another charge of the opposite polarity from the environment, forming an exciton

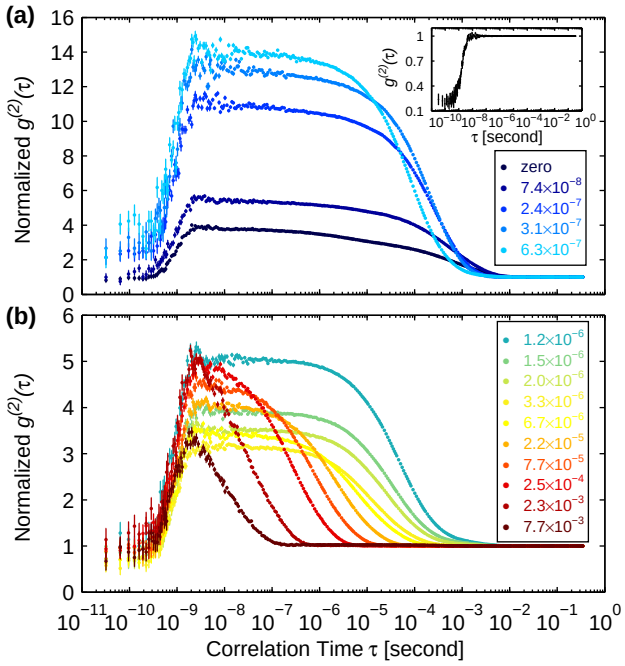

FIG. 5. (Color online) Second-order correlation function of the fluorescence, $g^{(2)}(\tau)$. The legends list the above-band laser power in fractions of the saturation power P_1. **(a)** The $g^{(2)}(\tau)$ measured at the black dots in box A in Fig. 3(d). The resonant laser is tuned to ∼1.96 GHz detuning with power of 0.1 P_0 and the above-band laser power is varied from zero to 6.32×10^{-7} P_1. A significant increase of bunching amplitude and small shrinking of bunching time can be seen. The inset is the correlation data measured with only above band-gap laser excitation at 0.23 P_1. **(b)** The $g^{(2)}(\tau)$ from box B in Fig. 3(d). The resonant laser is at ∼0.56 GHz detuning with a power of 0.1 P_0. The power of above-band laser is varied from 1.24×10^{-6} P_1 to 7.69×10^{-3} P_1.

and returning to a neutral condition. Thus the QD may switch between charged and neutral states, emitting resonance fluorescence while neutral and no fluorescence while charged. Therefore, the emitted photons will be bunched on a time-scale similar to the time it takes the QD to capture a charge.

Figure 5(a) and Figure 5(b) show how $g^{(2)}(\tau)$ is affected by the variations of the environmental free charge carrier density introduced by the above-band laser. All correlation data are normalized to the long time value at 0.2 seconds and plotted on a logarithmic time scale so both the short-time and long-time behavior can be clearly seen. All data show a clear dip near $\tau = 0$ and an exponential decay at longer times down to an asymptotic value. In a linear-log plot, an exponential decay is characterized by a high plateau followed by a sharp decay at the characteristic time of the exponential, finishing with another lower plateau. The dip is a sign of antibunching, and the decay is a sign of bunching, with the height of the plateau at intermediate τ values indicating the degree of bunching. Correlation functions like this indicate that

on short time scales the emitted photons are antibunched (*i.e.* two photons are unlikely to be emitted within one lifetime), but that on long time scales the photon stream is separated into bunches. The antibunching is expected of emission from a single QD, and the bunching indicates that there are phenomena that cause the QD to intermittently stop being excited by the resonant laser. Due to the finite response time of the detectors (∼0.8 ns), the bunching plateau is convolved with the anti-bunching dip to result in the measured $g^{(2)}(0) \geq 1$. This observation is further supported by the fact that a higher bunching plateau accompanies a larger $g^{(2)}(0)$ value. All $g^{(2)}(\tau)$ data presented here show not a single exponential decay, but multiple exponential decays with different characteristic times (10^{-7} s $\sim$ 10^{-2} s). These decays probably originate from both the charging of the QD and the fluctuation of the charge configuration of nearby traps, as discussed above.

To obtain the maximum signal-to-noise ratio in $g^{(2)}(\tau)$, we followed the brightest peak position in the RPLE map to collect the correlation data; the points of collection are marked by black dots in Fig. 3(d). Figure 5(a) shows the $g^{(2)}(\tau)$ results measured at the points in box A and Fig. 5(b) for those from box B. According to the fits to the RPLE data, when recording the correlations in Figs. 5(a) and 5(b) the resonant laser is mostly exciting the high energy peak of the fine structure doublet for either trap configuration (00) for box A or trap configuration (11) for box B.

As the above-band laser power increases, the bunching amplitude in Fig. 5(a) increases monotonically up to 14 due to the decrease of the probability of trap configuration (00) as indicated by the decreasing of fluorescence in Fig. 3(d). Bunching means that the overall emission is grouped into clumps of photons, and there is a dearth of photons between the bunches. An increase of the bunching amplitude reflects a reduction in the relative probability of detecting two photons separated by a long time interval. This indicates that the QD is turned into an "off" state or low count-rate state more frequently. If the QD turns "off" more frequently, it reduces the number of photon pairs with a long separation interval compared to those with a short separation interval. This unbalanced change leads to an increase of the relative probability to find a photon pair with a short separation interval, *i.e.* the increase of the $g^{(2)}(\tau)$ bunching amplitude. Pronounced intensity fluctuation (high bunching level) for the medium power regime in both Figs. 5(a) and 5(b) is associated with accelerated transitions between the different charge trap configurations. This leads to strong intensity fluctuations of the PL that monitors one of the particular configurations, *e.g.*, the (00) state for Fig. 5(a) and the (11) state for Fig. 5(b). This acceleration is reflected in the shortening of the characteristic decay time of the bunching in $g^{(2)}(\tau)$, from 10 ms to 1 ms for Fig. 5(a) and from a few milliseconds to a few microseconds for Fig. 5(b) up to the top of the high power regime.

In contrast to the decay time, in this power range (1.2×10^{-6} P_1 $\sim$ 2.5×10^{-4} P_1) the bunching amplitude shows a non-monotonic behavior. First it decreases from 5 to 3 when the above-band power increases up to 3.3×10^{-6} P_1, then it rises back up to 5 at 2.5×10^{-4} P_1, and finally it decreases again. The first decrease is due to the increasing probability for the traps to be in configuration (11), which is the charge configuration with which the laser is in resonance. In fact, an increase in PL at the same above-band power in the RPLE spectra gives a direct support for this argument; see Fig. 3(d). The following increase of bunching amplitude is associated with decrease of time-averaged total PL (Fig. 4(b)) in the same power range: the QD starts to capture another charge, and the neutral exciton emission becomes less favored while trion or biexciton population get correspondingly increased.

Fluorescence from the trion and biexciton are filtered out by the monochromator, and so do not contribute to the measured correlation. Therefore, one would expect a greater bunching amplitude for a higher above-band power. However, the opposite trend is observed in Fig. 5(b) when the above-band power is more than 2.5×10^{-4} P_1. It seems that the anti-bunching dip prevents the bunching amplitude from increasing further at short time scales. Physically this is because there are rarely photon pairs with time interval shorter than the lifetime of the QD. If the lifetime of the QD was shorter, one would expect the bunching amplitude to continue rising. In addition, the high density of free charge carriers in the ultra-high power regime enables both the QD and other sources (*e.g.*, the continuum tail of wetting layer defect states) to emit photons without resonant excitation. These extra photons would fill the gaps between the bunching of the resonant-excited-QD emitted photons, leading to a slight decrease of the anti-bunching dip depth and a decrease of the bunching amplitude.

As a comparison, we did a similar correlation measurement with only above band-gap excitation and found that there is no bunching at all for all the excitation powers used from 7.0×10^{-3} P_1 to 6.3 P_1 and the inset of Fig. 5(a) gives one example of those measurements at 0.23 P_1. Although that excitation power is far above the threshold for obtaining emitters aside from the QD, a well-defined anti-bunching dip down to 0.2 is still present. It is possible that the decrease of the dip depth in the resonantly excited correlations in Fig. 5(a) is mostly due to the finite response time of the detectors rather than simultaneous photons from multiple sources. Thus the resonantly excited QD even including its environment as a whole would still be a good single photon source at this point.

We note that several essential studies on closely related topics were published in the past few years, such as quantum dot charging[27] and nearby charge trap dynamics[28]. A brief summary of those works and a comparison to our study are provided here. The QD studied by Nguyen *et al.*[27] has an above band excitation saturation power of 30 μW, which is consistent with our value of 28.5

μW. They also note that their QD emits no resonance fluorescence without a particular very small amount of above-band laser power. This is similar in kind if not degree to our observation that the resonance fluorescence is a maximum with a non-zero above-band laser power. Without above-band excitation, Ngugen *et al.* extract a charge trap ionization and neutralization rate on the order of 10^4 s^{-1} while our results show a large range of bunching decay rates from 10^3 s^{-1} to 10^5 s^{-1}. This difference is probably due to the fact that our QD can emit resonance fluorescence without above-band excitation, leading to a $g^{(2)}(\tau)$ measuring both effects of QD ionization and charge trap dynamics. Nevertheless, this rate range is consistent with the study by Arnold *et al.*[28], where the trap loading/unloading rate varies from 4×10^3 s^{-1}to 6×10^4 s^{-1}, although their QD shows much larger discrete Stark shift ($\sim$18 GHz) indicating either a much larger QD dipole moment or a much closer charge trap. Nguyen *et al.* also extracted a QD charging rate of $\sim10^4$ s^{-1} at low above band power (0.01 nW), and of 10^7 s^{-1} at high above-band power (230 nW). Correspondingly at the same above-band power, our transition rate is $\sim10^4$ s^{-1} at 6.3×10^{-7} P_1 and $\sim10^8$ s^{-1} at 7.7×10^{-3} P_1. This is a difference of one order of magnitude at high above band power, which can be understood by noticing that our QD experiences two sources of fluctuation, charging of QD itself and ionization of nearby charge traps, while Nguyen's QD only experiences the former one. Thus, the fluctuation of nearby charge traps increases the bunching decay rate. From Arnold's study, the transition rate of the charge trap is found to be $\sim1.6\times10^6$ s^{-1} for resonant excitation at 230 nW. This value is too low to explain the rate difference between our study and Nguyen's study at high above band power. But it is possible that this number would be significantly higher when using above-band excitation rather than below band gap resonant excitation, and thus bridging the difference. Qualitatively, our $g^{(2)}(\tau)$ bunching decay rate shows a linear relationship with the above-band excitation power, which is consistent with the results of both Nguyen *et al.* and Arnold *et al.*. There the extracted transition rate is proportional to either the above-band power or the square root of the power, but at the powers of interest here the larger linear term dominates if all effects are present in the data. Two other works observing discrete Stark shifts are Houel *et al.*[29] using differential reflection spectroscopy and Hauck *et al.*[30] using differential transmission spectroscopy. Both studied a sample with a Schottky diode structure that is different from ours, but the values of the discrete shifts are close to those presented here. Moreover, their interpretation of the phenomenon involves charges trapped around the QD with a distance of $\sim$100 nm[29] or $\sim$30 nm[30], which is close to the result of our calculation shown in the next section.

IV. POSSIBLE TRAP LOCATIONS

A change in the local electric field such as that produced by a nearby charge trap will shift the resonance frequency of the neutral exciton via the quantum confined Stark effect. Knowing the Stark shifts experienced by the QD allows us to calculate the possible positions of the charge traps. The shift as a function of the change in local electric field, $\Delta\mathbf{F}$, is:

$$\Delta\nu = (-\mathbf{p}\cdot\Delta\mathbf{F} - (\boldsymbol{\beta}\Delta\mathbf{F})\cdot\Delta\mathbf{F})/h \tag{1}$$

where $\mathbf{p}$ is the permanent static dipole moment of the exciton in the QD, and $\boldsymbol{\beta}$ is its polarizability tensor[31]. Here we use typical values for the dipole moment[30] and polarizability[32] of self-assembled InGaAs QDs: $\mathbf{p} = e\times(0.2\text{nm})\hat{z}$, and $\beta_{xx} = \beta_{yy} = \beta = 4$ μeV/(kV/cm)^2. The polarizability is not isotropic because the QD is not spherically symmetric. Given the QD's pancake-like shape it has negligible polarizability in the z-direction, $\beta_{zz} = 0$. From these symmetry considerations, Eqn. 1 reduces to

$$\Delta\nu = (-p\Delta F_z - \beta(\Delta F_x^2 + \Delta F_y^2))/h \tag{2}$$

The change in electric field produced at the QD location by a single charge at relative position $\mathbf{r}_i$ is:

$$\Delta\mathbf{F}_i = \frac{1}{4\pi\epsilon_0\epsilon_r}\frac{-q_i}{r_i^2}\hat{\mathbf{r}}_i \tag{3}$$

where q_i is the charge, and $\epsilon_r = 13.1$ is the dielectric constant of GaAs.

By fitting the data in Fig. 3(a) we obtain 4 different values of the Stark shift, which we attribute to the 4 possible charge configurations of 2 nearby charge traps. We assume the charge configuration that is most likely with zero above-band laser power corresponds to the equilibrium configuration, (00), where both charge traps are neutral. We define the corresponding Stark shift to be zero: $\Delta\nu_0 = 0$ GHz. The other three Stark shifts are:

$$\begin{aligned}\Delta\nu_1 &= -3.3607\text{ GHz}\,(+0.0201/-0.0064\text{ GHz})\\ \Delta\nu_2 &= +1.1189\text{ GHz}\,(+0.1064/-0.0028\text{ GHz})\\ \Delta\nu_3 &= -2.2145\text{ GHz}\,(+0.1054/-0.0053\text{ GHz})\end{aligned} \tag{4}$$

where $\Delta\nu_1$ corresponds to configuration (10), $\Delta\nu_2$ corresponds to configuration (01), and $\Delta\nu_3$ corresponds to configuration (11). We make the assignment of $\Delta\nu_3$ to the doubly charged configuration because it corresponds to the predominant fluorescence peak at high above-band laser power. Both traps being charged is the most likely configuration when the above-band laser is producing many free charges that may be captured by the traps.

We can combine Eqns. 2 and 3 to determine the possible positions $\mathbf{r}_i$ that are consistent with the known values $\Delta\nu_i$ of the resonance shift. For a single charge trap this results in an equation that relates the distance r_i between the QD and the trap to the polar angle θ_i between the

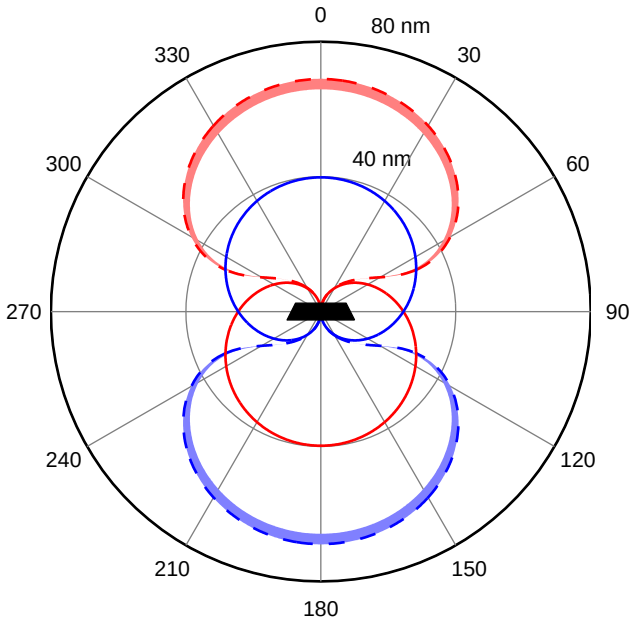

FIG. 6. (Color online) Possible charge trap locations consistent with the measured Stark shifts. Red and blue correspond to positive and negative trap polarity, respectively; the QD is represented schematically at the origin. The solid lines are for trap α; the dashed lines are for trap β. The shaded regions denote locations consistent with the confidence range of $\Delta\nu_2$; the confidence range of $\Delta\nu_1$ is small enough that the corresponding region is hidden by the solid lines.

$\hat{z}$-axis and the vector $\mathbf{r}_i$:

$$\Delta\nu_i = \frac{pkq_i}{hr_i^2}\cos\theta_i - \frac{\beta k^2 e^2}{hr_i^4}\sin^2\theta_i \qquad (5)$$

where $k \equiv 1/(4\pi\epsilon_0\epsilon_r)$ and q_i is the charge of the trap when ionized. Since the RPLE data cannot distinguish the polarity of the traps when they are charged, we do not know the sign of q_i. Thus, we consider both the case where the charged trap is positive ($q_i > 0$) and the case where it is negative ($q_i < 0$). Using the values and confidence intervals of $\Delta\nu_1$ and $\Delta\nu_2$ and Eqn. 5 we can determine the sets of possible values (r_1, θ_1) and (r_2, θ_2). Each set of possible positions defines an azimuthally symmetric volume in the space around the QD. Figure 6 shows colored areas which are cross-sections through these volumes for both possible polarities (red = positive; blue = negative) of trap α (solid lines) and trap β (dashed lines); a schematic of a typical 20 nm diameter QD is shown at the origin.

From Fig. 6 we can see that to cause the measured Stark shifts, a charge trap must be less than 70 nm away from the QD, which is relatively close: less than four QD diameters. Thus, any charge trap located at the DBR interfaces or surface is too far away to cause these discrete spectral shifts. Two charge traps within a spherical volume of radius 70 nm is consistent with the typical unintentional doping concentration of 10^{15} cm^{-3} for GaAs grown by molecular beam epitaxy. Notice that trap β must be either above or below the plane of the QD, depending on its polarity, while trap α could be above or below the QD plane regardless of its polarity. The separation between the resonantly excited QD and trap α is 30.6 nm if the trap is in the wetting layer (see Fig. 6). For comparison, in a sample with a high-density of self-assembled QDs[33] ($\sim$9.5$\times10^9$ cm^{-2}), the average dot-to-dot distance is about 103 nm, which is not much larger than the separation between the QD and trap α if it is in the wetting layer plane. Thus it is possible that trap α is another QD; however, this neighboring QD would be constrained to have only two charge states to be consistent with the RPLE data. Regardless of the identity of trap α, trap β cannot be another QD.

V. CONCLUSION

Resonant excitation spectroscopy successfully characterizes the local electric environment of the QD by providing detailed information about the number of nearby charge traps, their distances from the QD and their time-averaged occupation probability. Combined with weak above band-gap excitation below the level required to produce photoluminescence, the evolution of the local environment with respect to different densities of free charge carriers was studied, and we found that to achieve the maximum of total PL from the QD, a small amount of above-band excitation is required (Fig. 4(b)). This is similar to previous work on resonantly excited QDs[27,28,34–36], but here the behavior is more complicated. For the QD used in this study, the data indicate that there are two nearby charge traps within 70 nm. Their exact locations depend on the polarity of the trap when ionized, which the current measurement techniques are unable to determine.

Correlation measurements give information about the time-scale of switching from neutral to charged for both the traps and the QD. As the above-band excitation laser increases the density of free charge carriers, the time-scale of the charge trap dynamics speeds up, decreasing the switching time, which is reflected in the decay time-scale of the correlation bunching amplitude of resonantly excited fluorescence. This time-scale spans five orders of magnitude from 10^{-2} s to 10^{-8} s. Given the very long time-scales of bunching with zero or low above-band laser power, it is possible that many previous experiments did not recognize that the resonance fluorescence was bunched. We also note that the fastest bunching decay time of 10^{-8} s is only one order of magnitude longer than the anti-bunching time of about 10^{-9} s. In that case, the equivalent photon stream would be bunches of fewer than 10 photons, and long stretches of time with no emission between the bunches.

The combined techniques of resonant excitation spectroscopy and resonant fluorescence correlation can deter-

mine many details of the local charge environment of a single QD. The QD chosen for this work exhibits multiple spectral behaviors: discrete spectral jumps, continuous spectral shift, and spectral diffusion. These behaviors have been observed before by others, but the techniques demonstrated here allow quantitative investigation of the details. A QD that may be a suitable source of indistinguishable photons can be investigated using the same techniques to determine its potential.

ACKNOWLEDGMENTS

We would like to acknowledge C. Stephen Hellberg and T. Thomay for helpful discussions. GSS acknowledges partial support from the NSF PFC@JQI, and from Fulbright Austria-Austrian American Educational Commission through the Fulbright-University of Innsbruck Visiting Scholar program. This work was supported by the National Science Foundation (DMR-1452840).

* edward.flagg@mail.wvu.edu

[1] E. Knill, R. Laflamme, and G. J. Milburn, Nature **409**, 46 (2001).
[2] A. Zeilinger, M. A. Horne, H. Weinfurter, and M. Zukowski, Physical Review Letters **78**, 3031 (1997).
[3] J.-W. Pan, D. Bouwmeester, H. Weinfurter, and A. Zeilinger, Physical Review Letters **80**, 3891 (1998).
[4] D. L. Moehring, P. Maunz, S. Olmschenk, K. C. Younge, D. N. Matsukevich, L.-M. Duan, and C. Monroe, Nature **449**, 68 (2007).
[5] H.-J. Briegel, W. Dur, J. I. Cirac, and P. Zoller, Physical Review Letters **81**, 5932 (1998).
[6] Z. Zhao, T. Yang, Y.-A. Chen, A.-N. Zhang, and J.-W. Pan, Physical Review Letters **90**, 207901 (2003).
[7] C. K. Hong, Z. Y. Ou, and L. Mandel, Physical Review Letters **59**, 2044 (1987).
[8] P. Michler, A. Kiraz, C. Becher, W. V. Schoenfeld, P. M. Petroff, L. Zhang, E. Hu, and A. Imamoglu, Science **290**, 2282 (2000).
[9] C. Santori, M. Pelton, G. Solomon, Y. Dale, and Y. Yamamoto, Physical Review Letters **86**, 1502 (2001).
[10] A. V. Kuhlmann, J. H. Prechtel, J. Houel, A. Ludwig, D. Reuter, A. D. Wieck, and R. J. Warburton, Nature Communications **6**, 8204 (2015).
[11] C. Santori, D. Fattal, J. Vuckovic, G. S. Solomon, and Y. Yamamoto, Nature **419**, 594 (2002).
[12] O. Gazzano, S. Michaelis de Vasconcellos, C. Arnold, A. Nowak, E. Galopin, I. Sagnes, L. Lanco, A. Lematre, and P. Senellart, Nature Communications **4**, 1425 (2013).
[13] Y.-M. He, Y. He, Y.-J. Wei, D. Wu, M. Atatre, C. Schneider, S. Hfling, M. Kamp, C.-Y. Lu, and J.-W. Pan, Nature Nanotechnology **8**, 213 (2013).
[14] E. B. Flagg, A. Muller, S. V. Polyakov, A. Ling, A. Migdall, and G. S. Solomon, Physical Review Letters **104**, 137401 (2010).
[15] E. B. Flagg, S. V. Polyakov, T. Thomay, and G. S. Solomon, Physical Review Letters **109**, 163601 (2012).
[16] P. Gold, A. Thoma, S. Maier, S. Reitzenstein, C. Schneider, S. Hofling, and M. Kamp, Physical Review B **89**, 035313 (2014).
[17] H. D. Robinson and B. B. Goldberg, Physical Review B **61**, R5086 (2000).
[18] M. Abbarchi, F. Troiani, C. Mastrandrea, G. Goldoni, T. Kuroda, T. Mano, K. Sakoda, N. Koguchi, S. Sanguinetti, A. Vinattieri, and M. Gurioli, Applied Physics Letters **93**, 162101 (2008).
[19] M. Abbarchi, T. Kuroda, T. Mano, M. Gurioli, and K. Sakoda, Physical Review B **86**, 115330 (2012).
[20] A. V. Kuhlmann, J. Houel, A. Ludwig, L. Greuter, D. Reuter, A. D. Wieck, M. Poggio, and R. J. Warburton, Nature Physics **9**, 570 (2013).
[21] A. P. Beyler, L. F. Marshall, J. Cui, X. Brokmann, and M. G. Bawendi, Physical Review Letters **111**, 177401 (2013).
[22] C. Matthiesen, M. J. Stanley, M. Hugues, E. Clarke, and M. Atatüre, Scientific Reports **4** (2014), 10.1038/srep04911.
[23] S. Unsleber, D. P. S. McCutcheon, M. Dambach, M. Lermer, N. Gregersen, S. Hofling, J. Mork, C. Schneider, and M. Kamp, Physical Review B **91**, 075413 (2015).
[24] R. J. Warburton, C. Schäflein, D. Haft, F. Bickel, A. Lorke, K. Karrai, J. M. Garcia, W. Schoenfeld, and P. M. Petroff, Nature **405**, 926 (2000).
[25] M. Baier, F. Findeis, A. Zrenner, M. Bichler, and G. Abstreiter, Physical Review B **64**, 195326 (2001).
[26] J. J. Finley, P. W. Fry, A. D. Ashmore, A. Lemaitre, A. I. Tartakovskii, R. Oulton, D. J. Mowbray, M. S. Skolnick, M. Hopkinson, P. D. Buckle, and P. A. Maksym, Physical Review B **63**, 161305 (2001).
[27] H. S. Nguyen, G. Sallen, M. Abbarchi, R. Ferreira, C. Voisin, P. Roussignol, G. Cassabois, and C. Diederichs, Physical Review B **87**, 115305 (2013).
[28] C. Arnold, V. Loo, A. Lemaitre, I. Sagnes, O. Krebs, P. Voisin, P. Senellart, and L. Lanco, Physical Review X **4**, 021004 (2014).
[29] J. Houel, A. V. Kuhlmann, L. Greuter, F. Xue, M. Poggio, B. D. Gerardot, P. A. Dalgarno, A. Badolato, P. M. Petroff, A. Ludwig, D. Reuter, A. D. Wieck, and R. J. Warburton, Physical Review Letters **108**, 107401 (2012).
[30] M. Hauck, F. Seilmeier, S. E. Beavan, A. Badolato, P. M. Petroff, and A. Högele, Physical Review B **90**, 235306 (2014).
[31] R. J. Warburton, C. Schulhauser, D. Haft, C. Schaflein, K. Karrai, J. M. Garcia, W. Schoenfeld, and P. M. Petroff, Physical Review B **65**, 113303 (2002).
[32] B. D. Gerardot, S. Seidl, P. A. Dalgarno, R. J. Warburton, D. Granados, J. M. Garcia, K. Kowalik, O. Krebs, K. Karrai, A. Badolato, and P. M. Petroff, Applied Physics Letters **90**, 041101 (2007).
[33] A. Zolotaryov, A. Schramm, C. Heyn, and W. Hansen, Applied Physics Letters **91**, 083107 (2007).
[34] H. S. Nguyen, G. Sallen, C. Voisin, P. Roussignol, C. Diederichs, and G. Cassabois, Physical Review Letters **108**, 057401 (2012).
[35] M. Metcalfe, G. S. Solomon, and J. Lawall, Applied Physics Letters **102**, 231114 (2013).
[36] H. Nakajima, H. Kumano, H. Iijima, S. Odashima, and I. Suemune, Physical Review B **88**, 045324 (2013).